

Simplified approach for ductile fracture mechanics SSTT and its application to Eurofer97

Michael Mahler^{*}, Stephane Fessi, Jarir Aktaa^{*}

Karlsruhe Institute of Technology (KIT), Institute for Applied Materials, Hermann-von-Helmholtz-Platz 1, 76344 Eggenstein-Leopoldshafen, Germany

ARTICLE INFO

Keywords:

Small specimen testing technology
SSTT
Ferritic-martensitic
Crack-resistance curve
Crack growth
Fracture toughness
Ductile fracture mechanics approach
Eurofer

ABSTRACT

The determination of fracture-mechanical properties is often very challenging, because the available standards like ASTM E1820 need specific size-requirements for the specimen dimensions to obtain valid fracture toughness. Especially in the ductile regime, where the presence of plasticity around the crack tip is affected by the multiaxial stress state and its triaxiality, the size-requirements are frequently not met. The fulfilment of the size-requirements needs the testing of big specimens, which is often not possible. If we now think of specimens, which are irradiated in test modules for future fusion reactors, their size cannot be as big as required, because the available volume for irradiation is restricted. This fact highlights the need of Small Specimens Test Techniques (SSTT) for the determination of fracture-mechanical properties in the ductile regime.

The presented work focuses on an approach for the determination of fracture-mechanical properties in the ductile regime including stable crack growth and crack-resistance behavior. The authors have developed the initial approach some years ago and within this work the approach was simplified as much as possible. The basic idea of the approach is, that the crack growth can be simulated using Finite Element Method combined with a cohesive zone model. The cohesive zone model is a two parametric model, namely the cohesive stress σ_c and the cohesive energy Γ_c , which are identified on small specimens only. The new simplified approach was now validated on ferritic-martensitic steel Eurofer97 at room temperature.

In the past, the approach used complicated features like a CCD camera system and has now been simplified in a way that no CCD camera system is required. The main part of the approach is the identification of cohesive zone parameters (cohesive stress σ_c and energy Γ_c) on small specimens. The cohesive stress σ_c can be determined on notched round tensile specimens with different notch root radius to account for different stress states or stress triaxialities in the specimen. With dedicated Finite Element modelling a local fracture stress dependent on stress triaxiality can be identified. The cohesive energy Γ_c can be carried out by simulating the small fracture-mechanical specimen using the Finite Element Method combined with the cohesive zone model and parameter fitting to experimental results. The cohesive energy Γ_c is treated to be identified, if the simulated crack-resistance curve describes the experimental behavior.

After identification of these parameters, a big fracture-mechanical specimen can be simulated using the cohesive zone parameters already determined on small specimens. Finally, the crack-resistance curve of a big specimen can be predicted and a valid fracture toughness can be identified if the size-requirements of the big specimens are met. In case the requirements are not fulfilled, a bigger specimen geometry can be simulated until all size criteria are met. With this method, the testing of big specimens can be avoided. For the future there is a Round Robin exercise planned including defined test matrices to demonstrate the general applicability of the approach.

1. Introduction

The use of Small Specimen Test Techniques (SSTT) is an important issue since many decades due to the presence of various size-effects like

the geometrical size-effect. In the last decades several symposia focusing on SSTT have been held [1–4]. Especially for fracture-mechanical properties, the determination of fracture toughness in the ductile regime is a nightmare. The use of small specimens does not allow the determination of valid fracture toughness, because size-requirements

^{*} Corresponding authors.

E-mail addresses: M_Mahler@web.de (M. Mahler), jarir.aktaa@kit.edu (J. Aktaa).

<https://doi.org/10.1016/j.nme.2020.100799>

Received 1 January 2020; Received in revised form 21 July 2020; Accepted 11 September 2020

Available online 5 October 2020

2352-1791/© 2020 Published by Elsevier Ltd. This is an open access article under the CC BY-NC-ND license (<http://creativecommons.org/licenses/by-nc-nd/4.0/>).

Nomenclature			
Symbol	Unit Name	σ_Y	[MPa] effective yield strength acc. to ASTM E1820
Δa	[mm] crack growth	a_0	[mm] initial crack length
$\Delta a_{blunting}$	[mm] stretched length according to blunting	a_0/W	[-] pre-crack ratio
Δa_{corr}	[mm] blunting corrected crack growth	B	[mm] thickness
Γ_c	[N/mm] cohesive energy	b_0	[mm] remaining ligament $W - a_0$
ν	[-] poisson ratio	D	[mm] current diameter
ρ	[mm] current radius of curvature	D_0	[mm] initial diameter
σ_1	[MPa] principle stress, direction 1	E	[MPa] Young's modulus
σ_2	[MPa] principle stress, direction 2	h	[-] triaxiality
σ_3	[MPa] principle stress, direction 3	J_Q	[N/mm] preliminary J-Integral
σ_c	[MPa] cohesive stress	J_{Ic}	[N\mm] critical J-Integral mode I
σ_{multi}	[MPa] stress, multiaxial	J_{max}	[N\mm] maximum J-Integral capacity
σ_{uni}	[MPa] stress, uniaxial	K_{IIc}	MPa \sqrt{m} valid fracture toughness
σ_v	[MPa] von Mises stress	W	[mm] height
		CZM	Cohesive zone model

mentioned in fracture-mechanical standards like ASTM E1820 [5] are frequently not met. Due to this reason, the authors developed in the past an approach, which is able to cover the geometrical-size effect in case of

ductile fracture toughness. This approach is explained in details in [6,7] and [8]. The approach utilizes fracture-mechanical experiments combined with dedicated Finite Element modelling to describe the crack

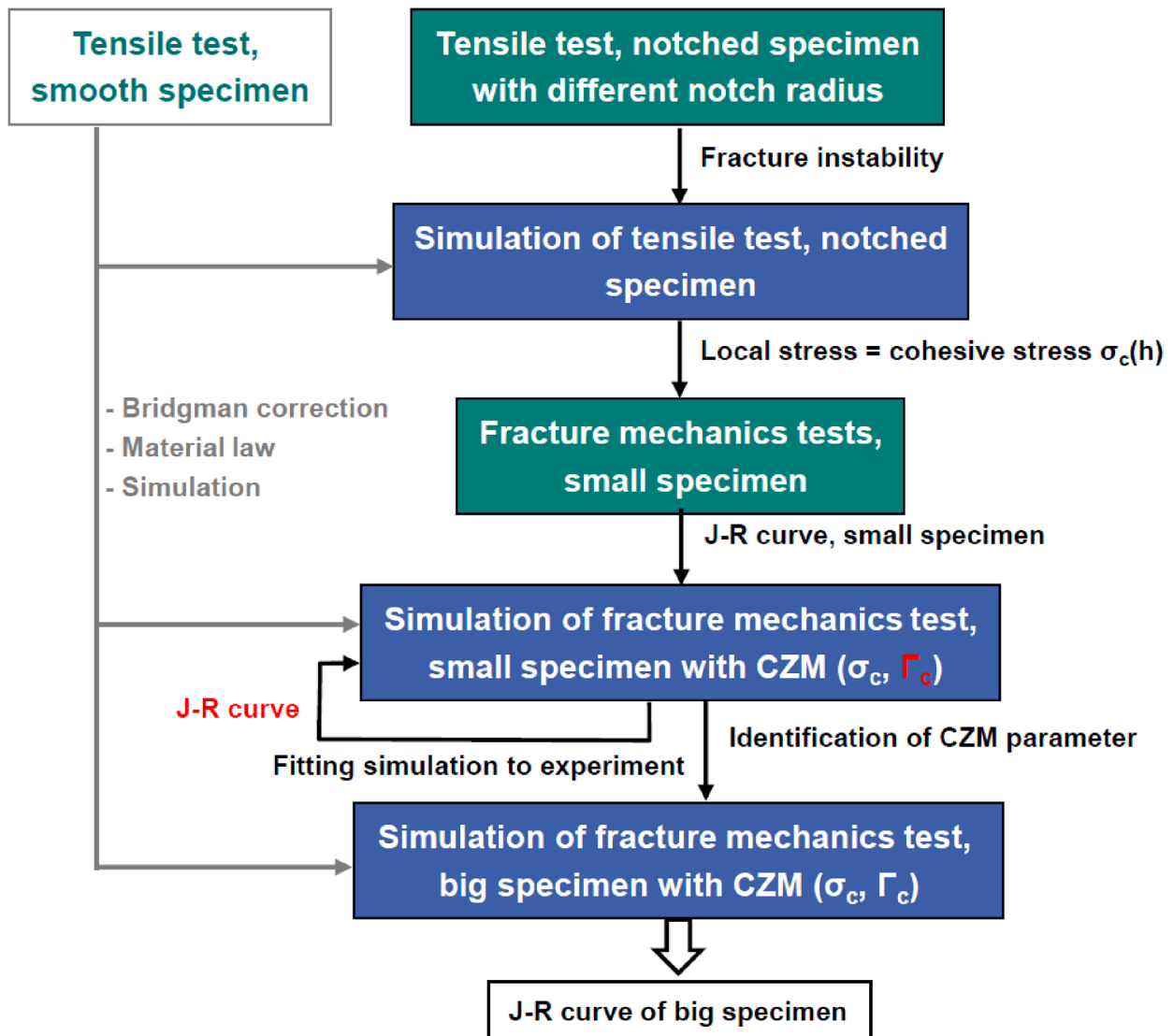


Fig. 1. Simplified ductile fracture mechanics approach.

growth of a small fracture-mechanical specimen. In a second step, the identified parameters coming from the small specimens were used to predict the crack growth of a big specimen. Finally, a crack-resistance curve can be predicted and - if the simulated specimen was big enough - a valid fracture toughness can be determined without experimental testing of the big specimen.

The approach, which the authors refers to in the present paper, is a simplified version of the original approach. The goal was to make the approach as simple as possible. The original approach uses for example a CCD camera system to observe the necking of the smooth tensile specimen and to calculate the average true strain at fracture of the notched tensile specimens. Now this has been replaced by using a limited number of interrupted smooth tensile specimens not tested until failure. For the notched tensile specimens, the determination of average true fracture strain is no longer required, because the fracture instability is identified directly from experimental force vs. displacement curve. Furthermore there were different notch root radii in the notched tensile specimens used to account for different fracture stresses dependent on the stress triaxiality.

The approach presented within this paper has been applied to ferritic-martensitic steel Eurofer97-2 with heat number 993391. It is well known, that the Eurofer97 heat 2 shows inhomogeneity in the as-received material [9] and for this reason an additional post heat-treatment has been performed. The normalization temperature for this post heat-treatment was set to 980 °C for 30 min and the tempering temperature was equal to 760 °C for 90 min. For both, the cooling was performed in air. After this post heat treatment we assume homogeneous material behavior. The quality of this heat treatment will be pointed out within the following experiments (scatter).

2. Simplified approach for ductile fracture mechanics SSTT

The approach in the present paper is a simplified version of the ductile fracture-mechanics approach, which the authors developed some years ago [6,7,10]. The main improvement of the simplified approach is that now the approach does not need specific experimental equipment like a CCD camera system for the detection of diameter reduction and necking.

The simplified approach is illustrated in Fig. 1 in more details. It starts with tensile test on smooth specimens, normally with a strain rate $\approx 10^{-3}$ 1/s, to identify the true stress vs. true strain curve. This material specific curve is mandatory for all dedicated Finite Element simulations. The CCD camera system for observation of necking has been replaced by utilizing interrupted tensile tests between necking and fracture.

After this preliminary test, the approach itself needs two experimental tests highlighted with green boxes (Fig. 1). Each experimental test is used to identify one of the two parameters needed for describing the crack growth in the Finite Element simulation including a specific triaxiality dependent cohesive zone model [11]. The first experimental test is a tensile test on notched specimens with a mean strain rate over the notched region similar to that of the test on smooth specimen. In the simplified approach, the fracture instability from experiment of different notch root radius must be identified and the simulation of the specimen geometry (blue box) helps to identify the local stress at fracture instability. This stress is treated to be equal to the cohesive stress σ_c . Compared to the old approach, no CCD camera system is required and the average fracture strain is not important.

The second experimental test is the fracture-mechanical test performed with a small specimen. From the experiment, the crack-resistance curve (J-R curve) can be obtained and allows the fitting of the crack growth simulation (blue box) to the experimental curve. After this step, the parameters for the cohesive zone model are identified based on tests, which have been performed on small specimens, only.

The identified parameters can now be used to simulate a big fracture-mechanical specimen (last blue box) and predict the crack-resistance curve of a big specimen. The predicted crack-resistance curve allows

the determination of preliminary J-Integral J_Q to be able to check the size criteria of relevant standards for fracture toughness like ASTM E1820 from which valid fracture toughness can be calculated. If the size-requirements are not met, a bigger specimen can be simulated and the size-requirements can be checked again.

3. Specimen geometries and experimental details

For the determination of the parameters, a minimum number of small specimen is required and explained in the following. For each temperature of interest, three small smooth tensile specimens should be tested. Two of these specimens were tested until failure and the remaining specimen was used for an interrupted test (between uniform elongation and fracture) to identify the behavior after necking. In addition, three notched tensile specimens per notch root radius are recommended to account for different stress states. In this work the authors used notch root radius of 0.2, 0.35 and 0.5 mm with notch depth of 0.5 mm fabricated by turning. With this set of notched tensile specimens, the cohesive stress σ_c dependent on stress triaxiality can be determined using in total nine notched tensile specimens. For the second cohesive zone parameter e.g. 9 fracture-mechanical specimens, like KLST specimens tested in multi-specimen method according to ASTM E1820, can be used. Here it is important to mention, that the approach is not limited to the presented specimen geometries and will work with other small specimen geometries, as well. The drawings of the smooth and notched tensile specimens as well as the drawing of the fracture-mechanical specimen are shown in Table 1 a)–c).

Within this paper, the approach has been validated using a big fracture-mechanical specimen to obtain crack-resistance curve leading to valid fracture toughness. The specimen is a compact tension specimen with 0.5-inch thickness (0.5T-CT) and the corresponding drawing is shown in Table 1 d). As a summary, the recommended specimen types are listed in Table 1 e).

4. Parameter identification using small specimens

This section starts with the determination of true stress vs. true strain curve on smooth tensile specimens in Section 4.1. Followed by the parameter identification for the cohesive zone model using small specimens. The cohesive stress σ_c is identified in Section 4.2 and the cohesive energy Γ_c in Section 4.3.

4.1. True stress vs. true strain curve using smooth tensile specimen

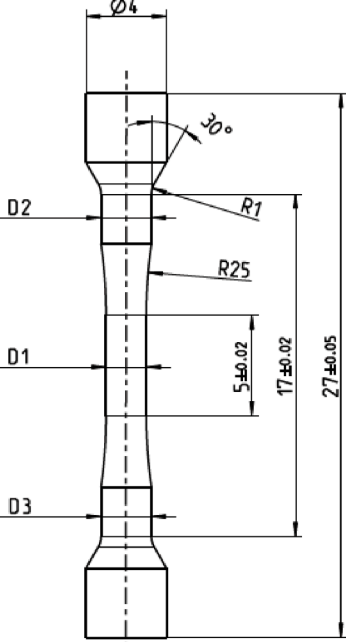
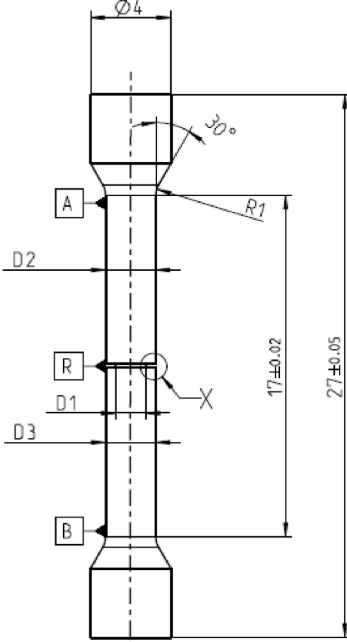
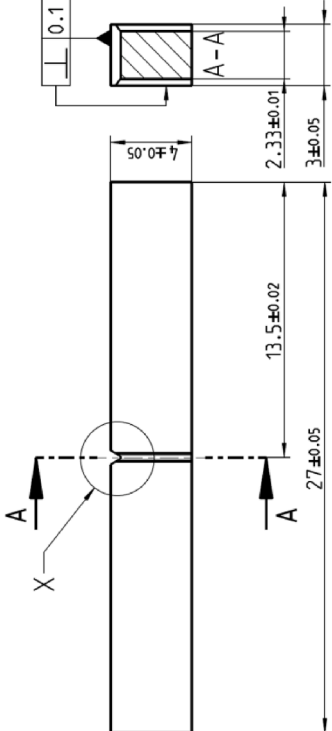
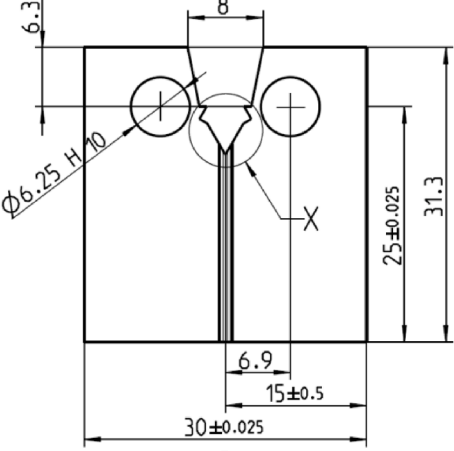
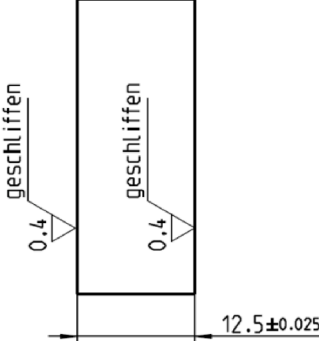
The true stress vs. true strain curve up to fracture is required as material input parameter for dedicated Finite Element simulations like the simulation of notched tensile specimen or the crack growth simulation. The curve can be obtained by performing a tensile test with a smooth tensile specimen. Due to the strain localization in the necking region, it is important to record the current diameter D to be able to calculate the true stresses and strains. With the onset of necking the uniaxial stress turns into a multiaxial one and the obtained stresses needs to be corrected utilizing the Bridgman correction [12], see Eq. (1):

$$\sigma_{uni} = \frac{\sigma_{multi}}{\left(1 + 4\frac{\rho}{D}\right) \ln\left(1 + \frac{1}{4}\frac{D}{\rho}\right)} \quad (1)$$

This correction requires the current radius of curvature ρ from the experiment. The original approach [6,7] used a CCD camera system to observe the current diameter and curvature during the whole experiment. Now the current diameters and curvatures are determined with interrupted tests and also with information after fracture for the specimens, which were tested until failure.

Fig. 2a) shows the experimental force vs. displacement of the smooth tensile specimens. Two specimens were tested until failure and one test was stopped shortly before fracture, to analyze the current diameter and

Table 1
Specimen geometries and test matrix.

small specimens		
 <p>a) tensile, smooth</p>	 <p>b) tensile, notched</p>	 <p>c) fract.-mech., KLST</p>
big specimen geometry for validation		Test Matrix
 <p>d) fract.-mech., 0.5T-CT</p>	 <p>e) specimen types</p>	<ul style="list-style-type: none"> - 3 tensile, smooth (plus interrupted tests) - 3 tensile, notched (per notch root radius) - 9 fract.-mech., KLST (multi-specimen method) - 3 fract.-mech., 0.5T-CT (single-specimen method)

curvature between necking and fracture. In a first step, the true stress vs. true strain was calculated up to the necking point at around 6% uniform elongation. Up to this point the true values can be calculated using simple formulae. In a second step, the diameter of the specimen coming from the interrupted test has been measured to calculate the corresponding true stress ($= 4F/(\pi D^2)$) and true strain ($= 2\ln(D_0/D)$), see grey triangle in Fig. 2b). A microscope image of the specimen from the interrupted test is shown in Fig. 3a). With the additional information of the curvature, the true stress has been corrected to be a uniaxial one using the Bridgman correction [12]. The corrected value can be seen

with black triangle in Fig. 2b). For the two specimens tested until fracture, the same calculation lead to the black rectangles in Fig. 2b). In summary, we have three data points for true stress and true strain between uniform elongation and fracture, namely:

- (1) Uniform elongation
- (2) Interrupted test
- (3) Fracture

In a final step these 3 points (marked in Fig. 2b) with purple color)

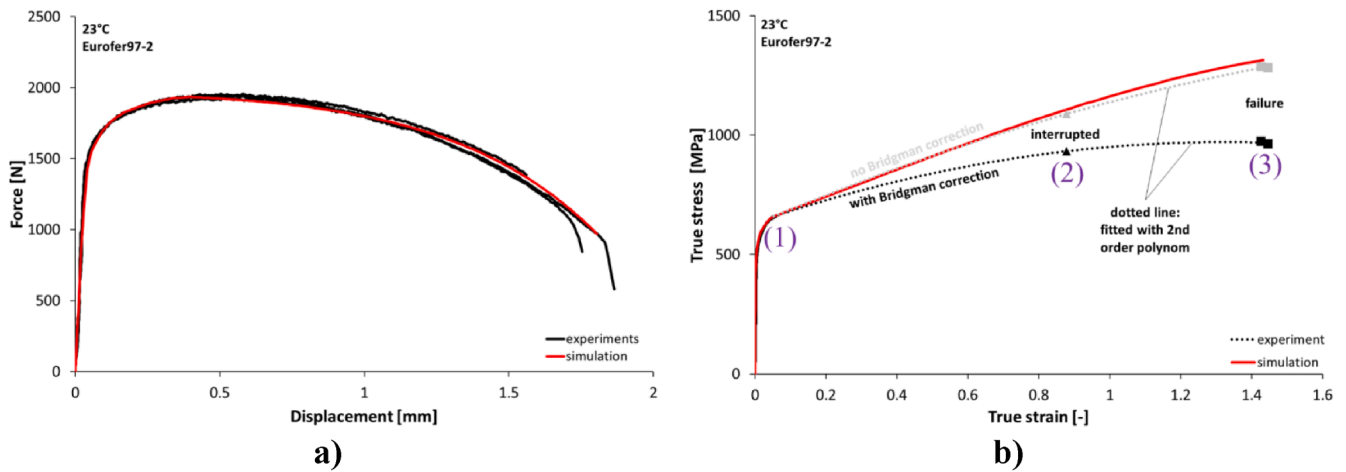


Fig. 2. Tensile test: a) force vs. displacement and b) true stress vs. true strain curve.

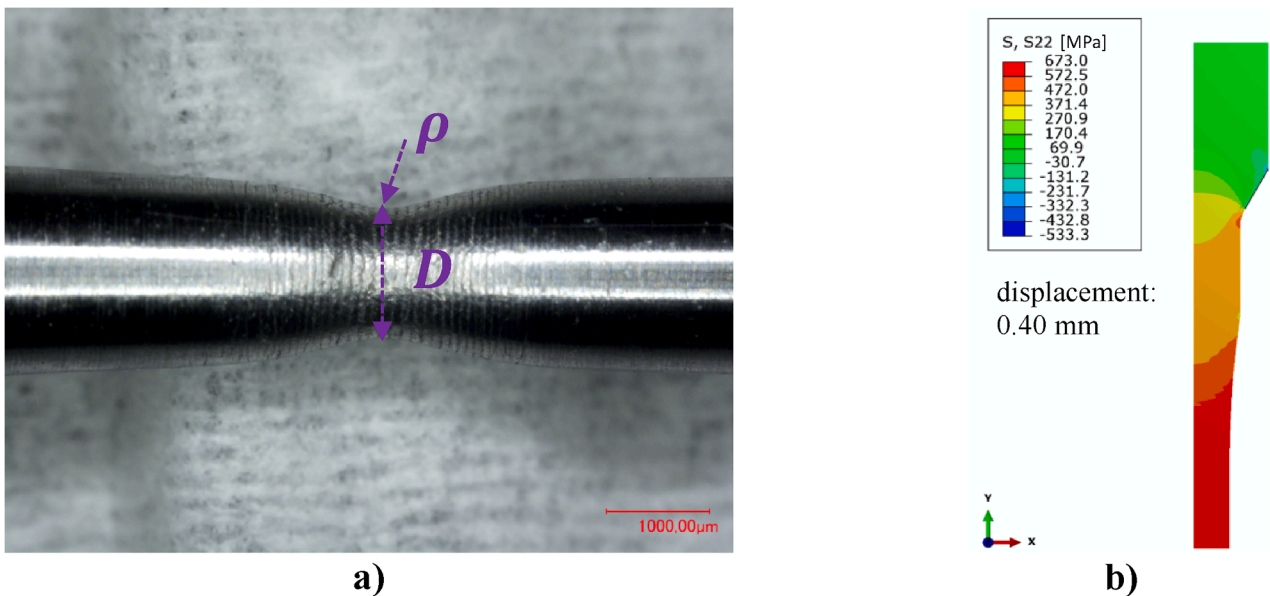


Fig. 3. Tensile test, smooth specimen: a) microscope image of interrupted test and b) simulation result of axial stress short before necking.

were fitted with polynomial function of 2nd order to be able to interpolate values. With this procedure, the true stress vs. true strain curve has been constructed and can now be used in dedicated FE modelling of the approach.

To guarantee that the obtained material data is correct, the tensile test has been simulated using the Bridgman corrected true stress vs. true strain curve as input parameter for the simulation. More details about how the FE simulation is conducted are published in [6]. The result of the Finite Element simulation is shown with the red color in Fig. 2a) and 2b). It is obvious that the simulation is able to describe the experiment and the true stress vs. true strain curve can be used. In Fig. 3b) the axial stress for a displacement of 0.4 mm (onset of necking) is illustrated and the stress distribution looks homogeneous. At fracture at around 1.82 mm displacement, the corresponding maximum axial stress reaches a value of 1487 MPa. This value will be used later in combination with the results on notched tensile specimens to determine the local fracture stress dependent on the stress triaxiality.

4.2. Fracture stress dependent on triaxiality using notched tensile specimen

After the determination of true stress vs. true strain curve, the approach starts with the experiments on notched tensile specimens, see first green box in Fig. 1. Notched tensile specimens according to Table 1 b) with a circumferential notch depth of 0.5 mm were tested with different notch radius of 0.2, 0.35 and 0.5 mm. The experimental results are illustrated with black curves in Fig. 4a)–c). This part is now the most important part of the simplified approach, because no CCD camera system is used to observe the diameter reduction of the notched tensile specimens. Only the fracture instability visible in force vs. displacement records is used as an identifier for fracture. A typical fracture surface can be seen in Fig. 4d).

For each notch radius, a Finite Element simulation has been performed. More details about how the FE simulation is conducted are published in [6]. Following the approach this part corresponds to the first blue box in Fig. 1. The specimens in the simulations were loaded up to the displacement from the experiment, where the fracture instability occurs (average of all tested specimens per notch root). This point is highlighted with a red rectangle in Fig. 4a)–c), respectively. At this

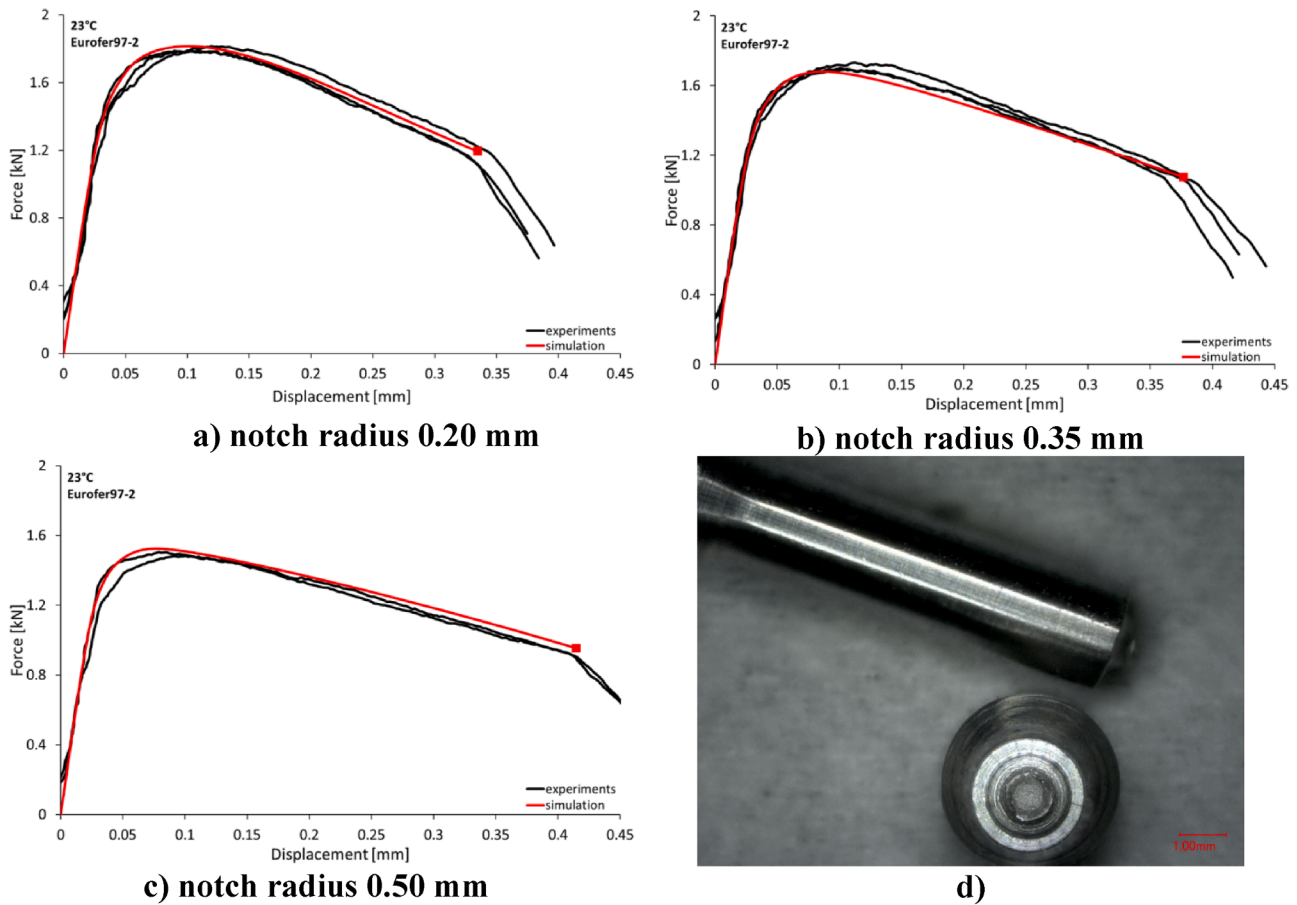


Fig. 4. Tensile test, notched specimen: Force vs. displacement curve with notch radius of a) 0.20 mm, b) 0.35 mm, c) 0.5 mm and d) microscope image after fracture.

deformation state, the maximum local axial stress is analyzed by FE post-processing. The highest axial stress (1839 MPa) was observed for the smallest notch radius of 0.2 mm. The other simulations yield a maximum axial stress of 1779 MPa for notch radius of 0.35 mm and 1752 MPa for 0.5 mm. For all simulations, the maximum axial stress moves during simulation from the notch tip to the center of the specimen and at fracture instability it has already reached the center of the specimen (see Fig. 5).

To address the influence of the multiaxial stress state within the specimen, the stress triaxiality h at fracture instability was calculated for each simulation. The stress triaxiality is defined as the ratio between the average of the principle stresses in the different directions divided by the von Mises stress, see Eq. (2):

$$h = \frac{\sigma_1 + \sigma_2 + \sigma_3}{3\sigma_v} \tag{2}$$

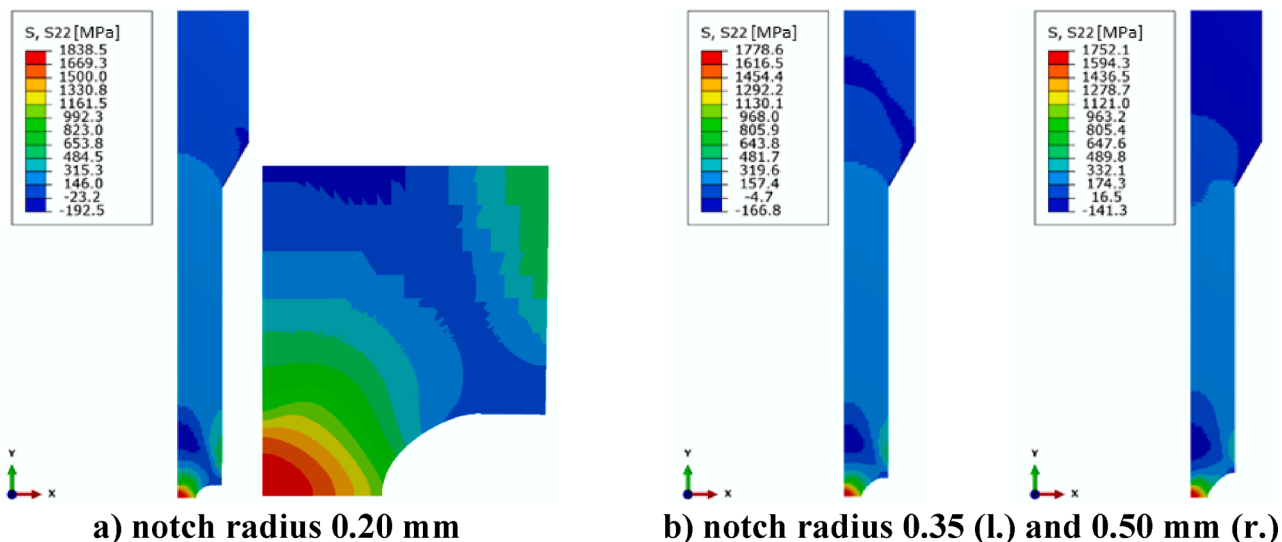


Fig. 5. Tensile test, notched specimen: Simulation result of axial stress at the onset of fracture for notch radius of a) 0.20 mm, b) 0.35 mm and c) 0.5 mm.

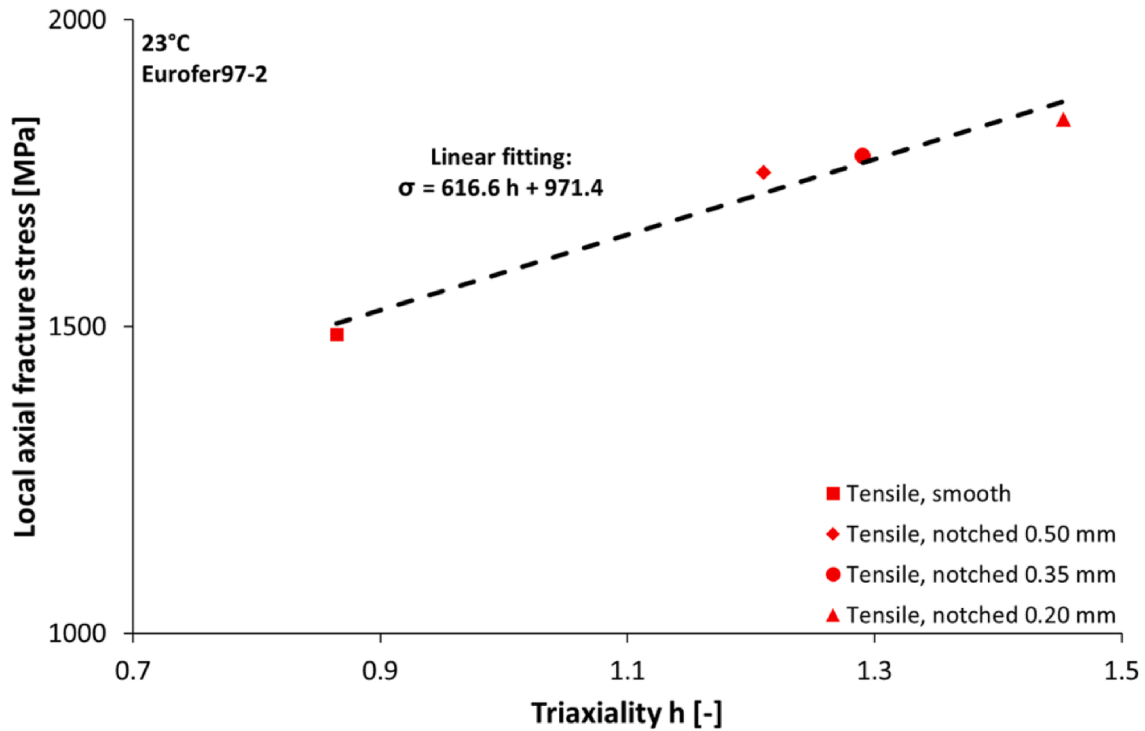


Fig. 6. Tensile test, notched and smooth specimen: dependence of local axial fracture stress on triaxiality.

The result is plotted together with the local axial fracture stress in Fig. 6. Not only the results of notched tensile specimens, but also the local axial fracture stress and triaxiality of the smooth tensile specimen is plotted in this diagram (red rectangle). The data points follow a linear relationship and can be fitted with the function in Eq. (3):

$$\sigma_c = c_1 h + c_2 \quad (3)$$

with c_1 and c_2 as material and temperature dependent parameters determined for Eurofer97-2 at RT equal 616.6 MPa and 971.4 MPa, respectively. This dependency of local axial fracture stress vs. triaxiality will be used as cohesive stress σ_c for the crack growth simulation. The introduction of a fracture stress dependence on the stress triaxiality allows to deal with the presence of the geometrical size effect. Therefore, its description by a proper function, here linear function (Eq. (3)), shall provide good approximation of fracture stress at stress triaxiality value in the range of those appearing in fracture mechanical specimens. How the second cohesive zone parameter, namely the cohesive energy Γ_c , can be identified is described in Section 4.3.

4.3. Small fracture-mechanical specimen

After the characterization of the dependency of cohesive stress σ_c on the stress triaxiality using small smooth and notched tensile specimens, the following step in Fig. 1 requires small fracture-mechanical specimens. The geometry of these fracture-mechanical specimens is not restricted. In this example, the so-called fracture-mechanical KLST specimen tested in three point bending was used. The KLST specimens have a pre-crack ratio a_0/W of 0.25 to allow stable crack extension of at least 1 mm and are side grooved with 20% total thickness reduction. This is necessary to guarantee a straight crack front, see fracture surface in Fig. 8a). Because of the small size of the KLST specimen measurements of crack opening displacement (COD) was not possible. Hence, to measure the crack-resistance curve at room temperature, nine specimens were tested according to ASTM E1820 using the multi-specimen method. The cross-head displacement rate during the experiment was 0.2 μm per second. The nine specimens were loaded up to different

deflections, to result in different crack growth. The obtained force vs. deflection curves are summarized in Fig. 7a) with black color. The low scatter in the shape of the curves show that the material behavior is homogeneous. The differences in maximum load are related to small variation in pre-crack ratios. The force vs. deflection curves together with the corresponding crack growth, which was measured with optical microscope (Fig. 8a)), can be used to construct the crack-resistance curve shown in Fig. 8b).

It is important to mention, that the tested specimens show a big blunting region before stable crack growth. In contrast to ASTM E1820 the authors did not count the blunting to the crack growth Δa and they did not draw a blunting line to account for blunting in the crack-resistance curve. The crack-resistance curve in Fig. 8b) uses a blunting corrected crack growth Δa_{corr} and it does not include the stretched length according to blunting [13]. The blunting corrected crack growth is defined according to Eq. (4) as:

$$\Delta a_{corr} = \Delta a - \Delta a_{blunting} \quad (4)$$

The crack blunting length $\Delta a_{blunting}$ was determined from the optical measurements. The experimental data points for the crack-resistance curve (black rectangle) were fitted with the following power function

$$J = J_1 \Delta a_{corr}^m \quad (5)$$

determining the material and temperature dependent parameters J_1 and m equal to 862.1 N/mm^{1+m} and 0.4898, respectively. The function fits the experimental values very well. This crack-resistance curve, the preliminary J-Integral J_Q can be determined without using the 0.2 mm blunting line (blunting corrected) and the value at 0.2 mm crack growth leads directly to the J_Q value.

In addition to the experiments, the approach (Fig. 1) requires the simulation of the fracture-mechanical specimen geometry. The Finite Element simulation has been performed using the elastic-plastic true stress vs. true strain curve from Section 4.1 in combination with a cohesive zone model [14] to describe the crack growth. The selected cohesive zone model is able to account for stress triaxiality [11]. For the cohesive zone model, the triaxiality dependent cohesive stress σ_c has

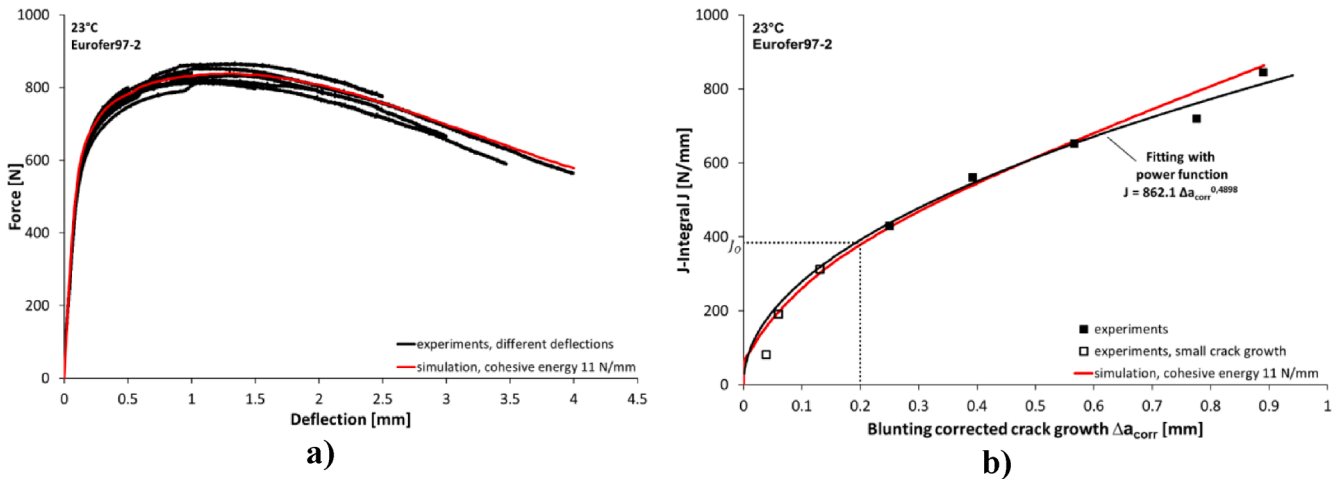


Fig. 7. Fracture-mechanical test, small specimen: a) force vs. deflection curve and b) crack-resistance curve.

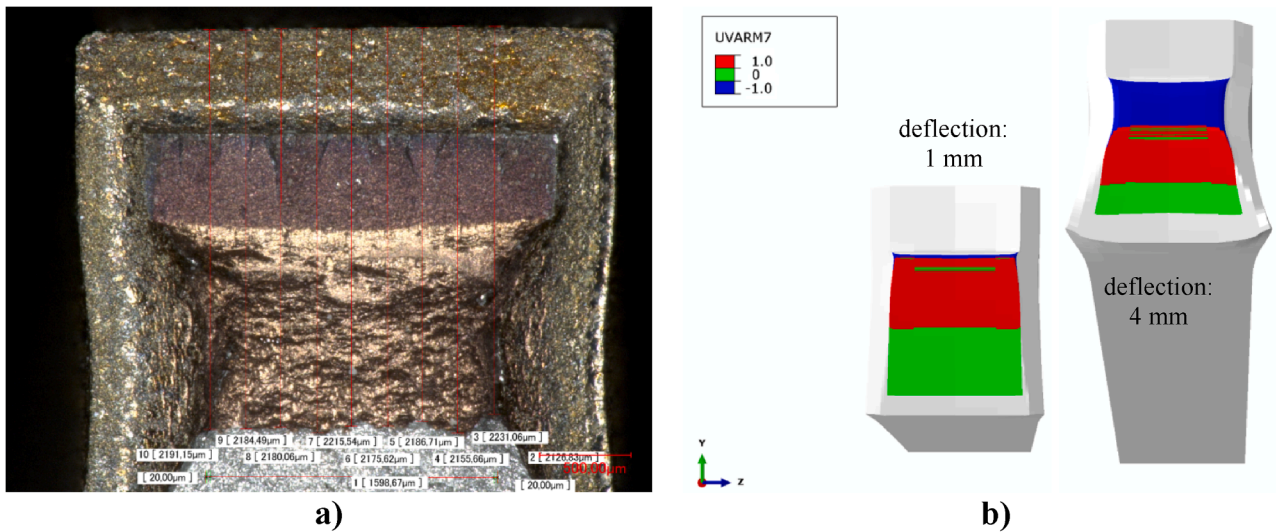


Fig. 8. Fracture-mechanical test, small specimen: a) heat tinted fracture surface showing stable crack growth after 4 mm deflection and b) simulated crack growth after 1 and 4 mm deflection (blue: separated/cracked area, red: loaded/stretched area, green: unloaded/compressed area).

been already determined in Section 4.2 and the only unknown parameter is the cohesive energy Γ_c . This parameter was determined by fitting the simulated crack-resistance curve to the experimental one. For a cohesive energy Γ_c of 11 N/mm the fitting yields a very good description of the experimental behavior, see red curves in Fig. 7a) and b). The simulation has used the average values of the specimen dimensions tested in the experiment like thickness B , height W , pre-crack ratio a_0/W . More details about how the FE simulation is conducted can be found in [6].

Fig. 8b) shows the simulated crack growth after 1 and 4 mm deflection. The area in blue shows the crack growth with broken cohesive elements as indicator for failure. The cohesive elements in red and green did not fail and the colors stand for elements under loading and unloading condition, respectively. A comparison of the experimental crack growth of Fig. 8a) and b) after 4 mm deflection shows, that the simulation is in addition able to describe the shape of the crack front.

In summary, the experiments on small fracture-mechanical specimens combined with dedicated Finite Element modelling are able to identify the cohesive energy Γ_c . Now, Section 5 will deal with the prediction of crack-resistance curve using the parameters determined in the current section on small specimens.

5. Prediction of valid ductile fracture toughness on large specimens

Finalizing the approach (Fig. 1), a big fracture-mechanical specimen can now be simulated to predict the fracture toughness using the parameters identified on small specimens. To show the independence of specimen geometry the big fracture-mechanical specimens is not of three-point bend type like the small one, but of compact tension type.

In this example, a 0.5T-CT specimen (Table 1) was chosen to predict the crack-resistance curve by Finite Element simulation. The simulation model of the compact tension specimen used a pre-crack ratio a_0/W of 0.5 and side grooves with 20% total thickness reduction. The Finite Element simulation has been performed comparable to the crack growth simulation of the small fracture-mechanical specimen utilizing cohesive zone elements [11] and the cohesive zone parameters identified in Section 4. The simulated crack-resistance curve is shown in Fig. 9 with red color.

To validate the predicted curve from the simulation, accompanying experiments on 0.5T-CT specimens were performed. The specimens were tested according to ASTM E1820 using single-specimen technique with partial unloadings. Four specimens have been tested and the experimental crack-resistance curves are presented in Fig. 9 with black

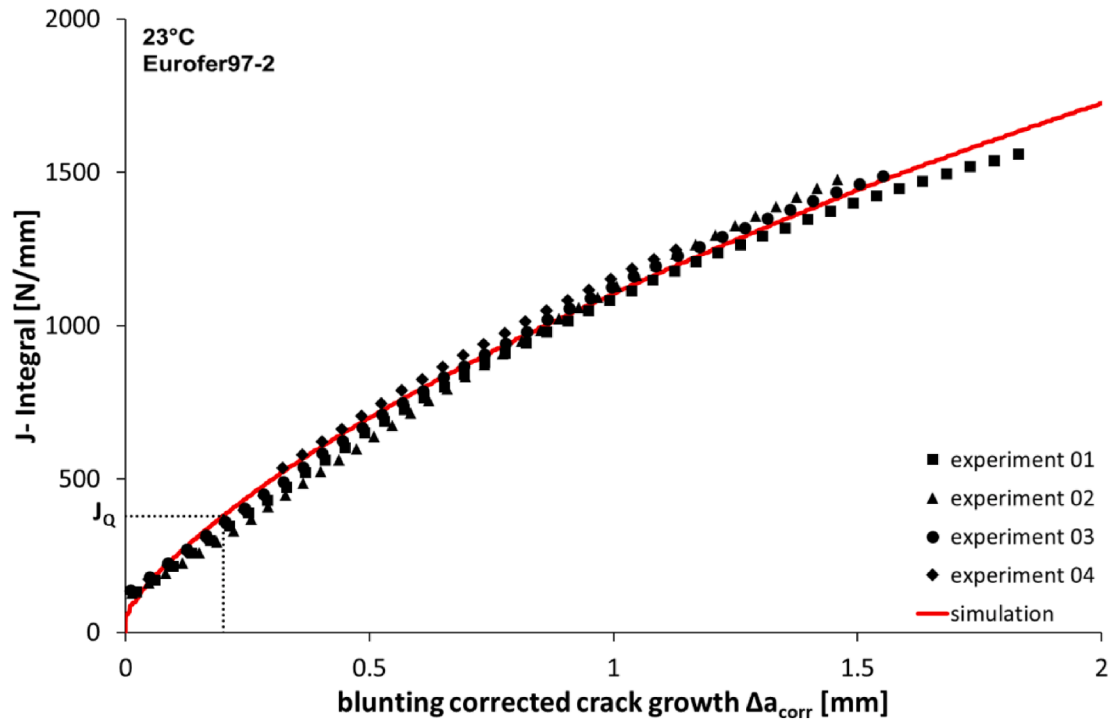


Fig. 9. Fracture-mechanical test, big specimen: crack-resistance curve.

color. There is a perfect agreement between predicted curve coming from the simulation and experiment.

Here it is important to mention, that the crack growth was blunting corrected. In case of single-specimen method the blunting corrected crack growth was not measured directly. It was calculated based on the experimental stiffness obtained for each unloading. The stiffness vs. unloading number in Fig. 10a) shows, that for the first 10 unloading there is more or less no change in stiffness (open rectangles) followed by a linear stiffness decrease (filled rectangles). The constant stiffness can be related to the effect of blunting. A comparison of measured initial crack length a_0 with electron microscope and calculated initial crack length (based on obtained stiffness) confirms, that the difference is equal to the visible blunting in the fracture surface shown in Fig. 10a). For this reason, the linear part after around 10 unloading was extrapolated back to the first unloading. The stiffness and calculated crack length a_0 obtained with this linear extrapolation is in very good agreement with the experimental initial crack length a_0 . The force vs. crack opening

(COD) curves coming from the experiments of the four tested 0.5T-CT specimens are shown in Fig. 10b) for completeness.

With this procedure, the approach was able to predict the experimental crack-resistance curve of a big specimen utilizing parameters coming from small specimens. Based on this, the preliminary J_Q and if size-requirements are met, the fracture toughness K_{JIC} can be calculated, finally.

6. Results and discussion

The simplified approach has been developed to reduce the complexity of the original approach [6]. The main goal was to avoid the use of additional measurement equipment like CCD camera system.

For the determination of true stress vs. true strain in Section 4.1 an interrupted test with only one tested specimen between uniform elongation and fracture has been used instead of using continuous measurement with a CCD camera system. In combination with a specific

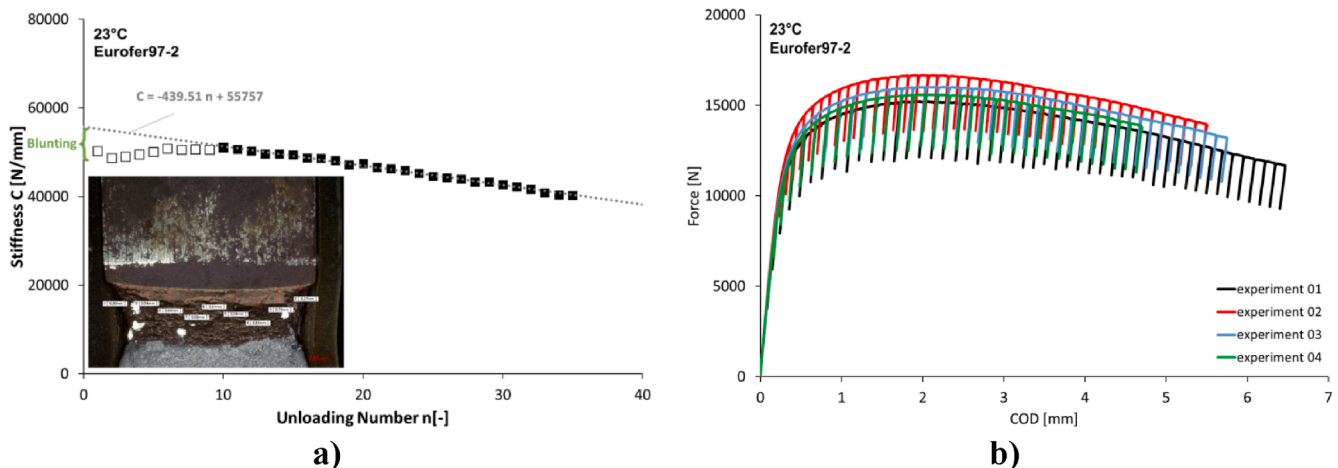


Fig. 10. Fracture-mechanical test, big specimen: a) example of stiffness vs. unloading (specimen N09) and b) force vs. COD curves of four tested 0.5T-CT specimens.

fitting procedure it was possible to construct the Bridgman corrected true stress vs. true strain curve. However the authors recommend to test a minimum of three specimens between uniform elongation and fracture instead of one single specimen. The use of one specimen might not work as good as demonstrated in this paper, particularly interrupting the test between uniform elongation and fracture. The quality of the obtained true stress vs. true strain curve can be validated with Finite Element simulation.

For the determination of the cohesive stress used in the cohesive zone model the procedure was simplified regarding notched tensile specimens, too. Now, the onset of fracture is directly identified by the force drop, which is visible in the experimental force vs. displacement curve. With dedicated Finite Element simulation the local true stress at fracture instability has been determined. Each family of notch radius lead to different maximum local true stress and corresponding triaxiality. These values were treated to be equal to the triaxiality dependent cohesive stress. In combination with the maximum local true stress and triaxiality coming from the smooth tensile specimen the stress triaxiality is characterized between stress triaxiality of 0.86 and 1.45, see Fig. 6. An extrapolation to a higher stress triaxiality in the range of sharp crack is possible with the obtained linear relationship in Eq. (3). A higher stress triaxiality means in general higher local fracture stress as long as there is plasticity. The triaxiality of a fracture-mechanical specimen will be between 2 and 3 and leads to high local fracture stresses.

The fracture-mechanical experiments on small specimens provided a crack-resistance curve which do not lead to valid fracture toughness. The preliminary J-Integral J_Q is equal to 392 N/mm. With this the size-requirements in ASTM E1820, see Eqs. (6) and (7) can be checked:

$$W - a_0 > \frac{10J_Q}{\sigma_Y} \quad (6)$$

$$B > \frac{10J_Q}{\sigma_Y} \quad (7)$$

The effective yield strength σ_Y in Eqs. (6) and (7) is defined as the average of yield and ultimate strength of the material at the temperature of interest. In this case the formulae requires a value of 6.8 mm and this cannot be fulfilled with the used KLST specimen and no valid fracture toughness can be obtained. However the crack-resistance curve was used for dedicated FE modelling to identify parameters to describe the crack growth. With a cohesive energy of 11 N/mm the simulation was able to describe the experimental crack-resistance curve in combination with stress triaxiality cohesive stress.

With the same cohesive zone parameters the simulation of a big fracture-mechanical 0.5T CT specimen predicts the crack-resistance curve shown in Fig. 9. From this curve the preliminary J-Integral J_Q is equal to 384 N/mm. This value is very similar to the one obtained with the small fracture-mechanical specimen (392 N/mm). The main difference is, that the small specimen does not fulfill the size-requirements. For the 0.5T-CT specimen the required specimen thickness B (without excluding the depth of side grooves according to ASTM E1820) and remaining ligament must be bigger than 6.7 mm. The 0.5T-CT specimen has a thickness B of 12.5 mm and the remaining ligament is also equal to 12.5 mm. Hence, the size-requirements are fulfilled and the preliminary J-Integral J_Q is equal to J_{Ic} , see Eq. (8).

$$J_{Ic} = J_Q \quad (8)$$

Another important value is the maximum J-Integral capacity J_{max} in ASTM E1820 (Eq. (9)):

$$J_{max} = \min\left(\frac{B\sigma_Y}{10}, \frac{(W - a_0)\sigma_Y}{10}\right) \quad (9)$$

For this specimen geometry and material the maximum capacity is equal to 641 N/mm. In summary the specimen can be used to determine valid fracture toughness. The formula in Eq. (10) lead to a fracture toughness of 312 MPa \sqrt{m} :

$$K_{Ic} = \sqrt{\frac{EJ_{Ic}}{(1 - \nu^2)}} \quad (10)$$

For validation of the predicted fracture toughness, accompanying experiments on 0.5T-CT specimens confirmed finally the simulated crack-resistance curve.

7. Conclusion

The simplified approach works very well without additional measurement system required during the experimental testing. The basis for the approach is the proper determination of the uniaxial true stress vs. true strain curve. The presented approach is able to deal with the geometrical size-effect and predicts the crack-resistance curve of a big specimen. This works, because the crack growth simulation uses parameters, which depend on the stress state. The stress triaxiality is the key parameter for the success of this approach. The main advantage of this approach is, that small specimens can be tested and based on their results the crack-resistance behaviour of a big specimen can be simulated to predict valid fracture toughness. The approach is very beneficial, because it is possible to simulate a big specimen geometry and check if the size-requirements are met or not. If they are not met, a bigger specimen can be simulated until all size-requirements are fulfilled.

In summary this approach enables the use of any small fracture-mechanical specimens showing ductile crack growth. It is verified for Eurofer97 at room temperature and shall be straightforward applicable to other materials and temperatures particularly where creep effect on ductile damage and fracture can be neglected. Especially for fusion relevant materials under irradiation this approach can now be applied to post-irradiation experiments in hot cells to obtain valid fracture toughness. In this context, the approach is a very good contribution to the development of Small Specimen Testing Technologies. In the future there is a Round Robin exercise planned to show the general applicability within different research units all over the world.

CRediT authorship contribution statement

Michael Mahler: Conceptualization, Methodology, Writing - original draft. **Stephane Fessi:** Investigation, Visualization. **Jarir Aktaa:** Supervision, Writing - review & editing.

Declaration of Competing Interest

The authors declare that they have no known competing financial interests or personal relationships that could have appeared to influence the work reported in this paper.

Acknowledgements

This work has been carried out within the framework of the EURO-fusion Consortium and has received funding from Euratom research and training programme 2014-2018 and 2019-2020 under grant agreement No. 633053. The views and opinions expressed herein do not necessarily reflect those of the European Commission.

References

- [1] W. Corwin, S. Rosinski, E. von Walle, *Small Specimen Test Techniques*, STP1329-EB, ASTM International, West Conshohocken, PA, 1998.
- [2] M. Sokolov, J. Landes, G. Lucas, *Small Specimen Test Techniques: Fourth Volume*, STP1418, ASTM International, West Conshohocken, PA, 2002.
- [3] M. Sokolov, *Small Specimen Test Techniques: 5th Volume*, STP1502, ASTM International, West Conshohocken, PA, 2009.
- [4] M. Sokolov, E. Lucon, *Small Specimen Test Techniques: 6th Volume*, STP1576, ASTM International, West Conshohocken, PA, 2015.
- [5] ASTM Standard E1820 - 2018, "Standard Test Method for Measurement of Fracture Toughness," ASTM International, West Conshohocken, PA, 2018.

- [6] M. Mahler, J. Aktaa, Approach for J–R curve determination based on sub-size specimens using a triaxiality dependent cohesive zone model on a (ferritic–martensitic) steel, *Eng. Fract. Mech.* 144 (2015) 222–237.
- [7] M. Mahler, J. Aktaa, Prediction of fracture toughness based on experiments with sub-size specimens in the brittle and ductile regimes, *J. Nucl. Mater.* 472 (2016) 178–185.
- [8] M. Mahler, J. Aktaa, Approach for determining fracture mechanical properties from tests on small size specimens at room temperature, *Proc. Mater. Sci.* 3 (2014) 434–439.
- [9] L. Piloni, C. Cristalli, O. Tassa, L. Bozzetto, E. Zanin, N. Bettocchi, Development of innovative materials and thermal treatments for DEMO water cooled blanket, *Nucl. Mater. Energy* 19 (2019) 79–86.
- [10] M. Mahler, *Entwicklung einer Auswertemethode für bruchmechanische Versuche an kleinen Proben auf der Basis eines Kohäsivzonenmodells*, KIT Scientific Publishing, Karlsruhe, 2016.
- [11] I. Scheider, “The Cohesive Model Foundations and Implementation, 2nd revised edition,” GKSS Research Centre Geesthacht, 2006.
- [12] P. W. Bridgman, *Studies in large plastic flow and fracture*, New York, Toronto, London: McGraw-Hill Book Company, Inc, 192.
- [13] E. Gaganidze, J. Aktaa, Use of the failure assessment diagram to deduce ductile fracture toughness of the RAFM steel EUROFER97, *Int. J. Press Vessels Pip.* 86 (6) (2009) 345–350.
- [14] K.-H. Schwalbe, I. Scheider, A. Cornec, *Guidelines for Applying Cohesive Models to the Damage Behaviour of Engineering Materials and Structures*, Heidelberg, New York, Dordrecht, Springer, London, 2013.